Chemical Engineering Journal 337 (2018) 300–311

Contents lists available at ScienceDirect

Chemical Engineering Journal

journal homepage: www.elsevier.com/locate/cej

Integrated aerobic granular sludge and membrane process for enabling municipal wastewater treatment and reuse water production

Li Wang[a,1], Wenzhong Liang[a,b,1], Wensong Chen[a], Wenxiang Zhang[a,*], Jiahao Mo[a], Kaiguo Liang[a], Bing Tang[a], Yi Zheng[c], Feng Jiang[d]

[a] School of Environmental Science and Engineering and Institute of Environmental Health and Pollution Control, Guangdong University of Technology, Guangzhou 510006, PR China
[b] South China Institute of Environmental Sciences, Ministry of Environmental Protection, Guangzhou 510655, China
[c] School of Environmental Science and Engineering, South University of Science & Technology, Shenzhen 518055, Guangdong Province, China
[d] School of Chemistry & Environment, South China Normal University, Guangzhou, China

ARTICLE INFO

Keywords:
Aerobic granular sludge (AGS)
Ultrafiltration (UF)
Nanofiltration (NF)
Membrane fouling
Reuse water

ABSTRACT

Aerobic granular sludge (AGS), as an aggregate of numerous self-immobilized functional microorganisms, has been recognized as an increasingly viable option for wastewater treatment and reuse water production. This study aimed at evaluating the application of AGS reactor as primary, ultrafiltration (UF) as secondary and nanofiltration (NF) as tertiary treatment for the treatment of municipal wastewater, focusing on determining the membrane fouling mechanism and reuse water production. AGS reactor, UF and NF exhibit high removal efficiency for COD (51.33%, 90.48% and 99.26%) and nutrients (53.63%, 94.84% and 98.06% total nitrogen, and 49.8%, 97.07% and 98.73% phosphorus), indicating that the integrated aerobic granular sludge and UF/NF process could provide high pollution removal and quality reuse water. As for filtration behavior of UF and NF, shear stress produced by agitation speed could significantly improve flux, due to the dispersion of pollutants. Besides, for AGS, improved simultaneous nitrification and denitrification by the internal anaerobic, anoxic, and aerobic structure and the richer biological community increased foulant removal, while the larger pore size and mature structure also reduced foulant deposition. Moreover, shear stress also diminished the total fouling resistance, reversible fouling and irreversible fouling, as well membrane cleaning efficiency was promoted, by controlling AGS deposition on membrane. In addition, the fouling mechanism of conventional floc sludge and that of AGS were deeply analyzed and respectively compared, from three aspects, namely, Scanning Electron Microscope (SEM), Attenuated Total Reflection Fourier Transform Infrared Spectroscopy (ATR-FTIR) and Atomic Force Microscope (AFM). Overall, the results demonstrated an alternative option for water treatment and reuse water production in an integrated AGS and membrane process.

1. Introduction

Aerobic granular sludge (AGS), as an aggregate of numerous self-immobilized functional microorganisms, has a diversified microbial communities and tightly compact structure [1,2]. In the course of activated sludge water treatment, AGS gradually comes into being under suitable cultivation condition and effectively ameliorate organic pollutant degradation and nutrient convention [3–5]. Compared to the conventional activated sludge, AGS possesses several superiorities: huge biomass (up to 20 g TSS L^{-1}), rich microbial diversity, simultaneous nitrogen and phosphorus removal, low sludge generation, excellent settling capability, and ability to withstand high organic load [6–8]. Granular sludge regarding the above characteristics therefore shows a promising future in the development of wastewater treatment technology.

As an efficient separation technology, due to the compact size, high efficiency and superior selectivity, membrane has been widely employed in water treatment, including membrane bioreactor (MBR), pollutant rejection, resource recovery, tertiary or advanced treatment and reuse water production [9]. In actual water engineering, microfiltration (MF) was adopted for bacteria and particles removal; ultrafiltration (UF) could reject proteins and colloids [10]; small organic matter (200 < relative molecular mass < 1000) was intercepted by nanofiltration (NF) [11]; reverse osmose (RO) can effectively remove

* Corresponding author.
E-mail addresses: zhangwenxiang1987@qq.com, zhangwenxiang@gdut.edu.cn (W. Zhang).
[1] Li Wang and Wenzhong Liang contributed equally to this work and should be considered co-first authors.

https://doi.org/10.1016/j.cej.2017.12.078
Received 9 October 2017; Received in revised form 14 December 2017; Accepted 16 December 2017
Available online 16 December 2017
1385-8947/

salts and produce high quality reuse water [12]. In municipal water treatment, UF and NF/RO was applicated for advanced treatment of biological treatment effluent and reuse water production. Nevertheless, during this process, UF was fouled by gel layer produced by activated sludge, microorganism and colloids, and pore blocking caused by dissolved substances and microorganism; the main foulants of NF was small organic pollutant and some inorganic substances [9,13].

Utilizing their advantages to reinforce process efficiency and overcome their intrinsic shortcomings, the combination of AGS and membrane could compose an integrated membrane process: AGS-UF-NF. Li et al. [14] studied the feasibility of AGS-UF process for treatment of municipal wastewater. Thanks to its internal anaerobic, anoxic, and aerobic structure and the richer biological community, in contrast to the conventional MBR, it reveals higher organic pollutant degradation, and better nitrification and denitrification capacity. Moreover, the membrane permeability and membrane cleaning efficiency also raised by 50% and 10%, respectively, since AGS exhibited a less membrane fouling than that of activated sludge [15,16]. Tay et al. [17] found that AGS-UF had similar treatment efficiencies to that of conventional MBR (above 99% COD removal). Nevertheless, the TMP increment and permeability loss caused by membrane fouling could be negligible. Besides, another bench-scale experiment reported that the UF in AGS-UF could raise 50% membrane flux [18,19] than conventional MBR. Moreover, a long-term operation (above 100 day) of AGS-UF discovered that without any need for physical cleaning, UF still exhibited a low fouling rate (below 0.1 kPa/day) [20,21]. To now, all reports about the integrated AGS and membrane process just focused on the UF performance, and no studies involved the integration membrane process.

In this study, an integrated AGS and UF + NF process was adopted to treat municipal wastewater and generate reuse water. To have an insight into its feasibility and operation efficiency, there are still some problems that need to be addressed: 1) Can UF effectively reject the AGS from the effluent of AGS reactor? 2) What is the fouling mechanism of UF? 3) Can NF purify the permeate of UF and generate high quality reuse water? Furthermore, in order to alleviate membrane fouling, some fouling control methods also need to be revealed: 1) What is the interaction between AGS-foulants and shear rate on UF and NF? Can shear rate effectively reduce membrane fouling? 2) What is the critical flux of UF and NF? How can AGS-MBR keep at low membrane fouling with high flux operation?

To address these issues, the current study encompasses a detailed investigation into filtration performance and fouling mechanism of the integrated AGS and UF + NF process for municipal wastewater treatment and reuse water treatment. The main research contents include 1) to reveal the foulants composition of UF and NF; 2) to describe the fouling type; 3) to clarify the gradual fouling process; 4) to study the effect of shear rate on AGS and membrane fouling; 5) to investigate the critical flux. On the other hand, Scanning Electron Microscope (SEM) was selected to inspect the microscopic morphology of fouled membrane. The aim of this study could identify the membrane fouling mechanism of integrated AGS and UF + NF process, as well as is expected to facilitate the potential application in the future.

2. Materials and methods

2.1. Materials

2.1.1. AGS reactor and effluent characteristics

The AGS reactor is designed and fabricated by our lab, and its detail information was shown in previous study [6]. The construction of high shear and internal hydraulic cycle provides an ideal environment for the formation and growth of granular sludge. In our previous study [6], as shown in Fig. 1, the mature granular sludge with compact structure, clear outline and various microbial species was taken shape after 42 days' cultivation. The granular sludge test fluid was the suspension of AGS and its main characteristic is shown in Table 1.

2.1.2. Membrane materials

According to the manufacturer's information, the properties of MICRODYN-NADIR GmbH used in this study are summarized in Table 2.

2.1.3. Membrane module

The dead-end filtration Amicon 8050 cell (Millipore, Billaica, USA) was deployed in this study. The internal diameter of the cell is 6.35 cm and its maximum volume is 50 L. The membrane was located at the bottom of the cell. The effective membrane area is 3.17×10^{-3} m^2. A constant pressure was furnished by filling the cell with nitrogen gas and the maximal pressure could reach 0.6 Pa, whereas permeate was collected afterwards in a tube placed on an electronic scale in order to calculate the permeate flux.

2.2. Experimental procedure

All experiments were conducted at a controlled room temperature of 20 °C. A new membrane was employed for each test unless the permeability of the used membrane could be fully recovered to ensure the same initial membrane conditions for the entire study. The membranes were soaked in deionized water for at least 24 h before use, and pre-pressured with deionized water for 0.5 h under a pressure of 0.2 MPa

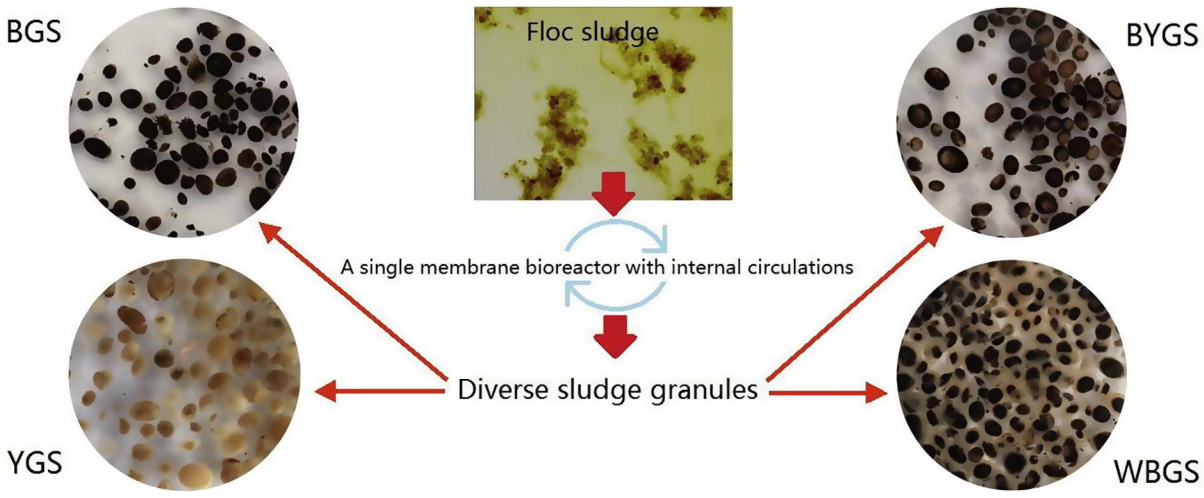

Fig. 1. Co-existence diverse sludge granules in AGS reactor. Figure reprinted from [22].

Table 1
Main characteristics of effluent of AGS reactor (mg/L).

COD	TP	NH_3-N	NO_2-N	NO_3-N
243.34	7.53	0.67	4.32	34.43

Table 2
Properties of MICRODYN-NADIR membranes tested.

Membrane	Surface material	Molecular weight cut-off (KDa)	Water permeability (L $m^{-2}h^{-1}$)[a]	Contact angle[b]
UP005	PES	5	30	73.6 ± 1.2
UP010	PES	10	150	74.6 ± 1.3
P010F	PESH	10	170	75.4 ± 1.5
UP020	PES	20	200	76.9 ± 1.8
UP030	PES	30	250	70.6 ± 1.8
UP100	PES	100	300	73.2 ± 1.5
NF270	PA	0.27	25–28	56.2 ± 2

PES, polyethersulphone. PESH, permanent hydrophilic polyether sulfone, PA, Polyamide.
[a] Own measurement at 20 °C and 0.3 Pa.
[b] The water droplet penetrates all the regenerated cellulose membrane during the measurements because they are highly hydrophilic.

for UF and 0.3 MPa for NF. After stabilization, the pure water flux of membranes was measured at 0.6, 0.5, 0.4, 0.3, 0.2 and 0.1 MPa for UF and 0.6, 0.5, 0.4 and 0.3 MPa for NF to calculate water permeability (Lp). Prior to the commencement of the experiments, the feed was heated to 35 °C, and was fully recycled in the system at zero TMP, and this process lasted about 10 min for each test. Then experiments were performed in two modes: full recycling tests and concentration tests.

2.2.1. Series 1: Full recycling tests

In order to estimate the membrane performance rapidly at various membrane types, agitation speeds and TMPs, these tests were performed with permeate and retentate recycling to limit the variation of feed volume to < 10%. A pre-filtration was carried out for 10 min at the lowest tested TMP and a rotating speed of 100 rpm, to ensure membranes stabilization. For each group of experiments, with the same membrane, TMP was augmented in steps from 0 to 0.6 MPa for UF and 0.2 to 0.6 MPa, but agitation speed was decreased in steps from 1200 rpm to 300 rpm except if stated otherwise. This procedure minimized the possible effect of concentration polarization or/and fouling formed at the previous test point on the next one, and the experimental protocol will be defined in more details later in each section. The filtration was periodically halted by suddenly releasing the pressure (0.05 MPa) so as to mimic back flushing and minimize the fouling accumulation from the last TMP step. Samples were collected in permeate 5 min after the beginning of each TMP increment or each agitation speed decrement for purpose of obtaining stabilized flux and transmission conditions.

2.2.2. Series 2: Concentration tests

In this section, 50 mL of test fluid was concentrated at a constant pressure and the permeate flux was recorded with time, while permeate was not recycled. The first 20 mL of permeate was discarded. When another 30 mL permeate was obtained, the filtration was stopped and permeate were collected for subsequent analysis.

2.2.3. Membrane cleaning

After each series of tests, the filtration system was flushed by deionized water for 10 min at 300 rpm. Then, alkaline cleaning was carried out by using a P3-ultrasil 10 (Ecolab, cleaning USA) detergent to remove foulants, at 0.25% concentration and 300 rpm, and Lp was measured to determine the permeability recovery.

2.3. Theoretical basis for threshold flux

With the purpose of achieving a sufficiently high flux in industry and keeping fouling rates at an acceptable range, Field and Pearce [23] defined “threshold flux”: “the threshold flux is the flux at or below which a low and near constant rate of fouling occurs, but above which the fouling rate increases markedly”. The threshold flux in membrane operation is affected to a great extent by fouling rate.

In previous study [24], threshold flux can be determined by flux-TMP profile and linear regression: a straight line of best fitting was drawn through stable flux points from the initial point to a certain point (as large as possible), while the coefficient of linear regression R^2 must be higher than 0.99, and threshold point was the last point in this regression line of best fitting. Hence, the abscissa and ordinate of threshold point (J_{thr}, TMP_{thr}) are the threshold flux and threshold TMP, respectively.

2.4. Resistance in series model

According to Darcy’s law, the permeate flux can be described by a resistance-in-series model:

$$J = \frac{TMP}{\mu(R_m + R_{fouling})} \quad (1)$$

where TMP is the transmembrane pressure (Pa), μ is the solvent viscosity (Pa s), R_m is the membrane resistance (m^{-1}), and $R_{fouling}$ is the total resistance resulting from various fouling types (m^{-1}).

In this section, the intrinsic membrane, reversible fouling layer and irreversible fouling layer resistances were calculated as follows: (1) the intrinsic membrane resistance was calculated from the water permeability of the new membrane before experiment; (2) the sum of intrinsic membrane, reversible fouling layer and irreversible fouling layer resistances were attained from the water permeability of the fouled membrane after experiment; (3) the sum of intrinsic membrane and irreversible fouling layer resistances were obtained from the water permeability of the fouled membrane after membrane cleaning. Thus, the reversible fouling and irreversible fouling resistances were calculated according to Eq. (1).

2.5. Analytical items

General evaluation of the pollutant removal was carried out by comparing the discrepancy of the water quality indexes in both the feed and the permeate. Regular parameters, including COD, NH_3-N, NO_2-N, NO_3-N, and TP were chosen as the reference parameters. All the above parameters were measured on the grounds of the standard methods [25].

2.6. Membrane characterization

For the membranes before and after experiment, their variation in morphology during the process was inspected via SEM (SN-3400, Hitachi Ltd., Japan), ATR-FTIR (660-IR, Varian, Australia) and AFM (XE-100, Park System, Korea). The membrane weight was measured using an Electronic Scales (FA2004, China).

2.7. Calculated parameters

The rejection (R, %) was calculated according to the following equation:

$$R = \left(1 - \frac{C_p}{C_f}\right) \times 100\% \quad (2)$$

where Cp and Cf represented the water quality indexes in permeate and feed (average value during filtration process), respectively.

Permeability recovery (%) was defined by a comparison of the

average water permeability for cleaned and new membranes:

$$\text{Permeability recovery} = \frac{L_{pc}}{L_{pi}} \times 100\% \quad (3)$$

where L_{pc} and L_{pi} are water permeability ($L\,m^{-2}h^{-1}$) of the cleaned/fouled and new membranes, respectively.

At Amicon cell, the flow field is similar to Bodewadt flow filed [26]. On the circular membrane plane, shear stress on the membrane reaches the highest at the critical radius. Above the critical radius, shear stress is produced by free vortex. Below the critical radius, shear stress is generated by impeller vortex. The critical radius (r_c, m) was determined by the following equation [27,28]:

$$r_c = \frac{0.521N}{100 + 42.5N} \quad (4)$$

where N is agitation speed (rpm).

Average shear stress (τ_{av}, Pa) was defined according to the following equation [27,28]:

$$\tau_{av} = 0.0742N^{1.5}(r_c^{1.6} - 138r_c^3) \quad (5)$$

Average shear rate (γ_{av}, s^{-1}) was determined by the following equation [27,28]:

$$\gamma_{av} = 82.9N^{1.5}(r_c^{1.6} - 138r_c^3) \quad (6)$$

2.8. Data analysis

All full recycling tests were repeated at least three times, and concentration tests were repeated at least two times. The errors were controlled below 5%. Mean values were calculated and presented on the Figures and Tables.

TMP-flux profile data were accommodated to threshold flux model. The data were analyzed by nonlinear regression using Origin 8. Statistical analyses were undertaken through one-way ANOVA and significant differences for comparisons of treatment occurs if with $p < .05$.

3. Results and discussion

3.1. The performance of UF

3.1.1. The effect of membrane

Fig. 2(a) illustrates the flux of six UF membranes. It is manifest that flux for the six UF membranes increases in the following order: UP005 < UP010 < P010F < UP020 < UP030 < UP100, which could be explicated by a combination of pore size and porosity. On account of larger pore size and greater porosity, the membrane with higher MWCO exhibited lower inherent filtration resistance and greater flux [29]. What's more, due to its larger pore size, more solutes and particles in feed solution permeated through membrane, decreasing concentration polarization and fouling layer accumulating on membrane surface. In theory, for the large membrane pore size, the foulant particles easily enter the pores and lead to higher pore blocking fouling. However, the size of AGS exceeds than that of UF pore, thus more foulant particles were rejected on membrane and pore blocking reduced. Additionally, membrane surface properties also imposed affect upon flux performance. Compared with UP010, P010F with the same pore size indicated a higher flux, due to its effective surface modification and better anti-fouling capacity. As for UP030, its pore size was much smaller than that of UP100, but, unexpectedly, its flux exceeded the flux of UP100 above 8 min. Besides, as shown in Table 2, the hydrophilicity of UP030 is higher than those of other membranes. For

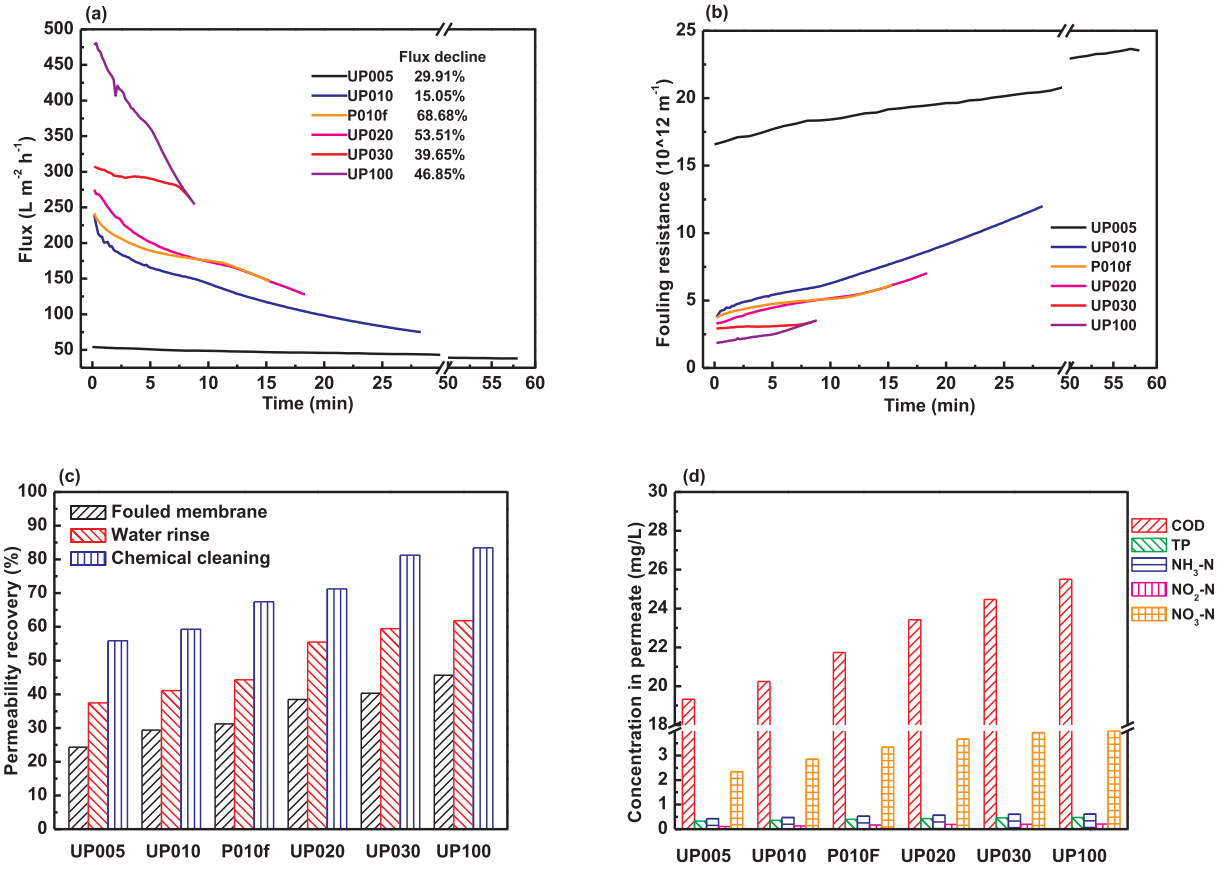

Fig. 2. Fouling behavior at different membranes: (a) Flux, (b) Fouling resistance, (c) Membrane cleaning efficiency and (d) Pollutant concentration in permeate (operation condition: 500 rpm agitation speed and 0.3 MPa TMP).

Table 3
Fouling resistance at different membrane.

Membrane	UP005	UP010	P010F	UP020	UP030	UP100
Fouling resistance (m^{-1})	16.58×10^{12} ~23.54×10^{12}	3.76×10^{12} ~12.00×10^{12}	3.71×10^{12} ~6.26×10^{12}	3.27×10^{12} ~7.02×10^{12}	1.87×10^{12} ~3.53×10^{12}	1.39×10^{12} ~4.01×10^{12}

high concentration polarization situation, UP030 exhibited an excellent antifouling capacity, which maybe on the surface its smaller pore size and modified surface had a smaller adsorption affinity with foulants and lower pore blocking.

The relationship between fouling resistance and time is presented in Fig. 2(b). The fouling resistance for all membranes are acquired from Table 3: $16.58 \times 10^{12}\,m^{-1}$ ~$23.54 \times 10^{12}\,m^{-1}$ (UP005), $3.76 \times 10^{12}\,m^{-1}$ ~$12.00 \times 10^{12}\,m^{-1}$ (UP010), $3.71 \times 10^{12}\,m^{-1}$ ~$6.26 \times 10^{12}\,m^{-1}$ (P010F), $3.27 \times 10^{12}\,m^{-1}$ ~$7.02 \times 10^{12}\,m^{-1}$ (UP020), $1.87 \times 10^{12}\,m^{-1}$ ~$3.53 \times 10^{12}\,m^{-1}$ (UP030) and $1.39 \times 10^{12}\,m^{-1}$ ~$4.01 \times 10^{12}\,m^{-1}$ (UP100). UP005 reveals the highest fouling resistance, whereas UP030 possesses the lowest fouling resistance. For all membranes, with the increment of time, more foulants accumulated on membrane and fouling resistance raised. As for the membrane with small pore size, most foulants in feed were intercepted, while high foulant concentration on membrane surface occurred, enhancing concentration polarization, fouling layer and high fouling resistance. With the enlargement of membrane pore size, the porosity increased and intrinsic resistance diminished. Besides, for the membrane with lager pore size, more organic matter could pass through membrane, indicating lower foulant concentration on membrane surface and reducing concentration polarization. P010F exhibits a higher fouling resistance than UP010, which is in accordance with Fig. 2(a). As for UP030, its fouling resistance was highly low, even equaled to UP100 after 8 min, which for the whole process, it almost kept constant.

As illustrated in Fig. 2(c), membrane fouling (irreversible) and cleaning efficiency are displayed by permeability recovery after water rinse and chemical cleaning. The permeability recoveries of all fouled membranes were lower than 50%, implying that numerous foulants deposited on/into membrane surface, and serious pore blocking and cake layer came into being. With the shrink of membrane pore size, the permeability of fouled membrane decreased, as a result of the high concentration polarization and fouling resistance, which was in line with the aforementioned analysis. In water rinsing, some foulants with loose structure can be cleared up and the permeability was regained to some extent. After that, P3-ultrasil 10 (Ecolab, USA) detergent, including EDTA, gluconate, phosphate, sulfate, NaOH and surfactant, were utilized for chemical cleaning [30]. Chemical cleaning could remove some organic foulants with stubborn structure, such as proteins and enzymes, and microbial, so the permeability recovery restored. Of course, for all membranes, the permeability could not be completely recovered, since some “stubborn foulants”, still adsorbed on/into membrane pores, could not be effectively removed by P3-ultrasil 10. For UP030 and UP100, their reversible fouling accounted for 19.13% and 16.20%, and were removed by water rinsing, thus after water rinsing, permeability recovery promoted from 40.32% and 45.64% to 59.45% and 61.84%, respectively. Then, after chemical cleaning, their permeability recoveries were up to 81.23% and 83.46% respectively, indicating that only about 21.78% and 21.62% foulants belonged to irreversible fouling. In general, larger membrane pores show higher permeability recovery and lower irreversible fouling, because of lower concentration polarization during filtration process. But for UP030, its permeabilities recovery after water rinse and chemical cleaning exceeded UP100, on account of high anti-fouling capacity by surface modification.

Fig. 2(d) shows the pollutants concentration in permeate for different membranes. All six UF membranes have high pollutant removal efficiency. Compared with the pollutant concentration in feed (the effluent in AGS reactor), the COD (19.33–25.68 mg/L), TP (0.33–0.51 mg/L), NH_3-N (0.43–0.64 mg/L), NO_2-N (0.11–0.23 mg/L) and NO_3-N (2.34–4.66 mg/L) in permeate have a relatively low concentration. In UF of the effluent of AGS reactor, most of sludge existed in a form of granular, and a majority of granular sludge indicated a much larger size than membrane pore, therefore, the granular sludge could be easily rejected by membrane. Although the pollutant concentration in sludge was very high, due to high rejection of granular sludge by membrane, the permeate demonstrated a very low pollutant concentration. Besides, the cake layers on membrane surface generated by granular sludge had a secondary rejection capacity and reinforce pollutant rejection. Furthermore, contrast to other membranes, both UP100 and UP030 exhibit high flux, stable pollutant removal and remarkable membrane cleaning efficiency, which proves to be an ideal selection for AGS reactor-UF application.

3.1.2. The effect of agitation speed

Fig. 3 presents the influence of agitation speeds on the filtration performance of AGS reactor. It is well known that shear rate on membrane surface reinforces with higher agitation or rotating speed [31,32]. As presented by Fig. 3(a), the high shear rate curtailed concentration polarization and membrane fouling, thus promoting permeate flux and decreasing fouling resistance obviously, especially for high TMP. Moreover, Fig. S1 shows that the threshold flux also improves with agitation speed, resulting from the reinforce of shear-induced back diffusion caused by high shear rate, particularly for granular sludge with large size (size > 100 nm) [30]. On the other hand, high shear rate also facilitated the recombination of some macro-pollutant particles [10,33], thus with high shear rate, small granular sludge turned into large granular sludge, which accelerated shear-enhanced back transport. Threshold TMP also raised with shear rate, on the grounds that high shear rate promoted the membrane anti-fouling capacity, and rebated the critical point for distinguishing fouling rate. Furthermore, as displayed in Fig. 3(b), at low agitation speed, with low shear-induced back diffusion, more foulants deposited onto membrane and fouling resistance raised. In addition, high flux also exacerbated fouling resistances, since more foulants were pushed onto membrane by high flux, giving rise to high concentration polarization and more serious foulants deposition.

Fig. 3(c) illustrates that the membrane cleaning efficiency at different agitation speeds. Elevating shear rate not only lessened the total fouling resistance, but also reduced irreversible fouling resistance and improved permeability recovery after membrane cleaning. This was on account of the diminishment of adsorption fouling caused by high shear rate.

As for the pollutant removal, the Table 4 shows that COD, NH_3-N, NO_2-N, NO_3-N and TP reveal highly low concentration in permeate. All COD and TP rejections are higher than 99%, and NO_2-N, NO_3-N and TP exceed 94%. NH_3-N exhibits a relatively lower rejection 45%–85%, due to its low feed concentration, in fact all NH_3-N concentrations are below 0.4 mg/L. Besides, with the amplification of shear rate, pollutant rejection by membrane reduced, as higher shear rate diminished the thickness of fouling layer, which exerted a “secondary” filtration effect on pollutant separation, thus the pollutant rejection curtailed. Therefore, it is concluded that a high shear rate on the membrane enables a reduction in fouling and generates a higher threshold flux.

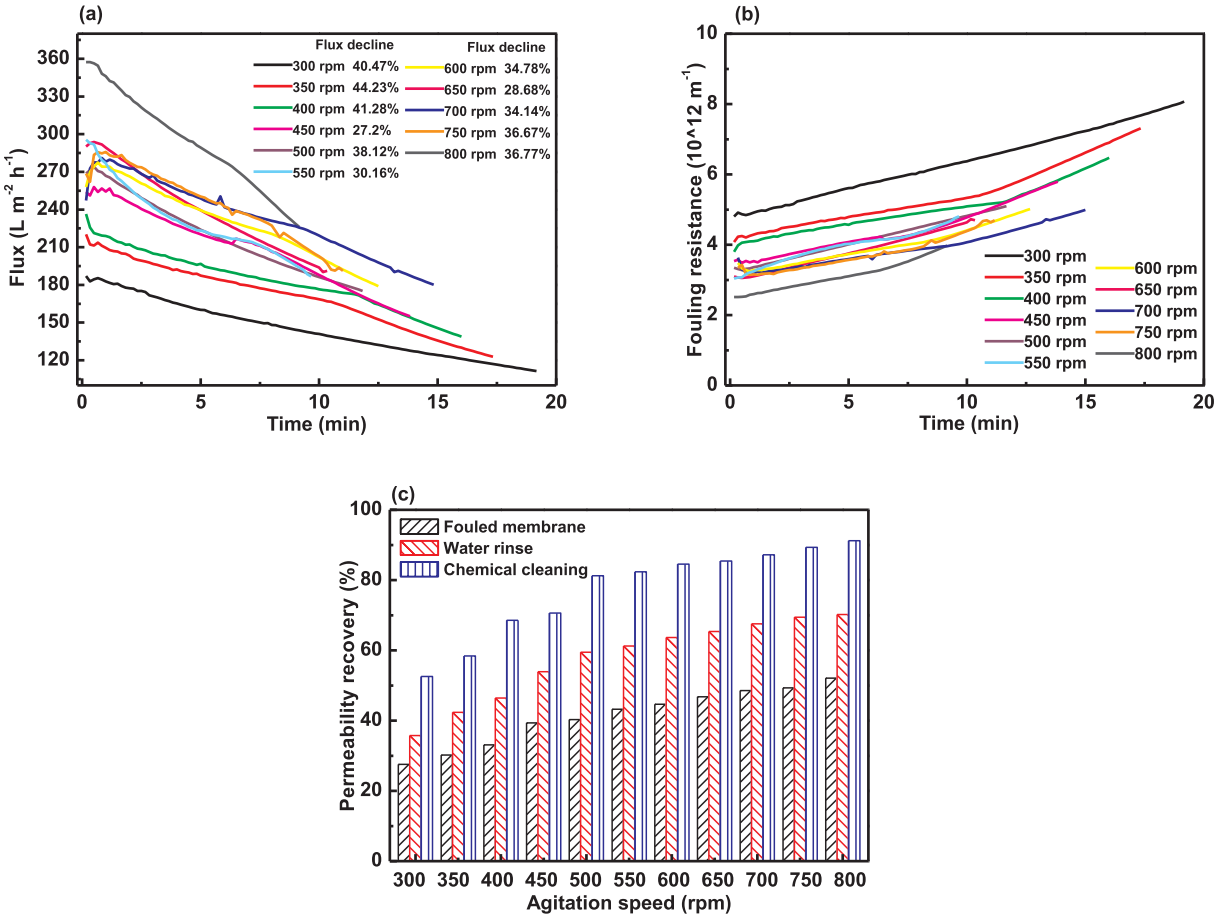

Fig. 3. Fouling behavior at different agitation speeds: (a) Flux, (b) Fouling resistances and (c) Membrane cleaning efficiency (operation condition: UP030 at the speed of 0.3 MPa TMP).

Table 4
Pollution removal at different shear stresses.

Agitation speed (rpm)	COD (mg/L)	TP (mg/L)	NH_3-N (mg/L)	NO_2-N (mg/L)	NO_3-N (mg/L)
300	21.24	0.32	0.09	0.19	3.23
350	21.45	0.34	0.12	0.21	3.35
400	21.57	0.41	0.18	0.23	3.48
450	22.26	0.43	0.19	0.25	3.58
500	23.18	0.44	0.24	0.26	3.89
550	23.59	0.47	0.26	0.28	4.04
600	24.12	0.50	0.28	0.31	4.09
650	24.34	0.52	0.31	0.35	4.15
700	25.02	0.53	0.35	0.36	4.24
750	25.11	0.54	0.38	0.37	4.27
800	25.23	0.58	0.39	0.38	4.32

Table 5
Pollution removal at different TMPs.

	COD (mg/L)	TP (mg/L)	NH_3-N (mg/L)	NO_2-N (mg/L)	NO_3-N (mg/L)
0.1 MPa	21.26	0.33	0.61	0.19	3.52
0.2 MPa	21.64	0.37	0.64	0.22	3.68
0.3 MPa	23.25	0.48	0.67	0.25	3.99
0.4 MPa	25.15	0.57	0.69	0.29	4.18
0.5 MPa	26.17	0.63	0.73	0.35	4.39
0.6 MPa	27.87	0.66	0.77	0.37	4.48

3.1.3. The effect of TMP

Table 5 demonstrates the influence of TMP on pollutant removal with the UP030. The concentrations of COD, NH_3-N, NO_2-N, NO_3-N and TP slightly elevate with TMP, stating that high TMP weakens the membrane rejection ability. As a matter of fact, the improvement of flux promoted by TMP plays a dual role in suppressing or encouraging separation efficiency [4]. At low flux, its increment could push more water molecular into permeate, which imposed a “dilute” effect and curtails pollutant concentration. On the other hand, when flux increased to a certain value, its continue increment could enhance concentration gradient of granular sludge and diffusive effect transfer through the membrane. In this section, the effect of flux on separation rate belonged to the latter reason. The augmented flux created by greater TMP elevated the transmission of small granular sludge and exerted a negative influence upon separation efficiency.

Fig. 4 illustrates the various fluxes, fouling resistances and membrane cleaning results at different TMPs. In Section 3.1 and Fig. 4(a) and (b), as expected, TMP intensifies the driving force and raises flux [34]. Higher TMP operation also enhanced the fouling resistance. After membrane cleaning, as illustrated in Fig. 4(c), the permeability recovery recedes with TMPs. These phenomena state that operating at higher TMP enlarged fouling resistance and irreversible fouling, which could be explicated as follows: high TMP and high flux pushed more granular sludges towards membrane surface, then promoted concentration gradient and more granular sludges deposited and formed fouling layer [35], thus enhancing membrane fouling.

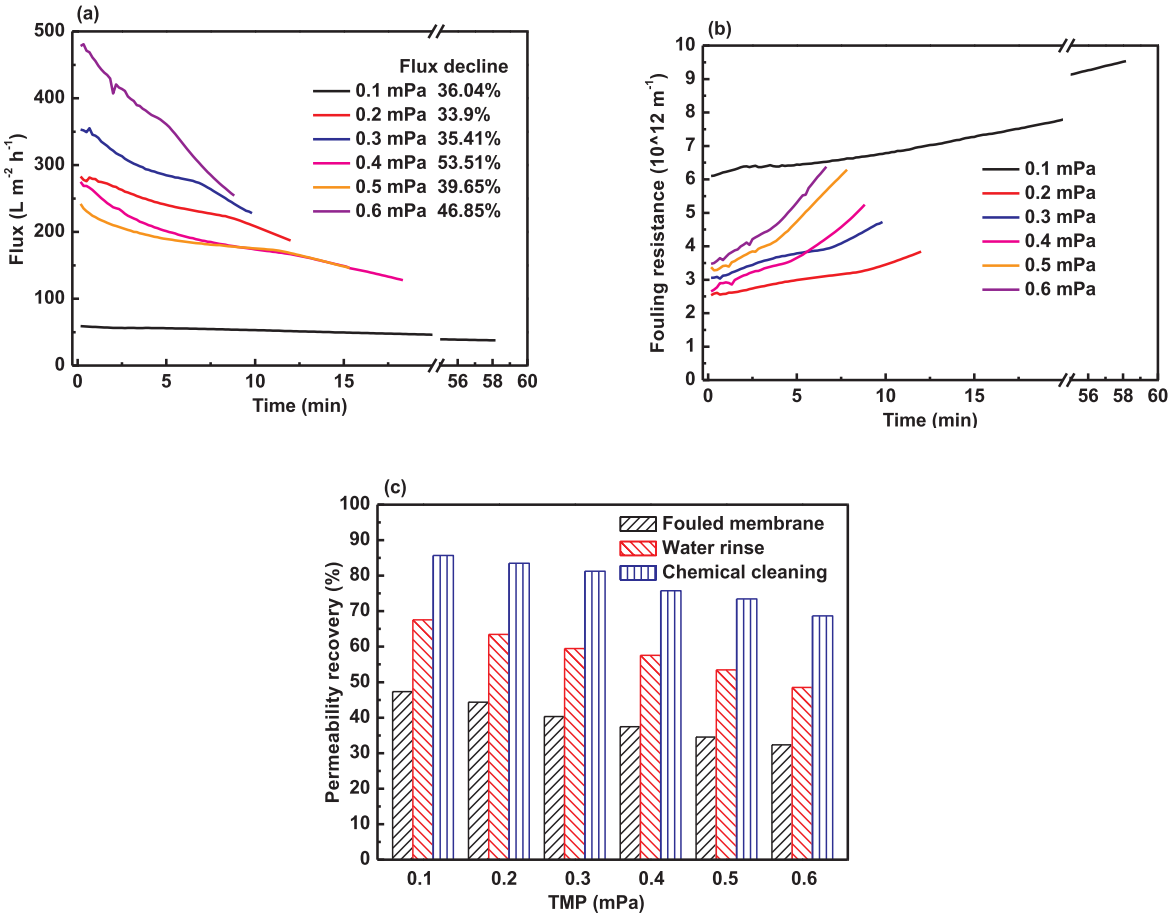

Fig. 4. Fouling behavior at different TMPs: (a) Flux, (b) Fouling resistances and (c) Membrane cleaning efficiency. (operation condition: UP030 at the speed of 500 rpm agitation).

3.2. The performance of NF

3.2.1. The effect of agitation speed and TMP

Fig. 5 shows the effect of agitation speed on permeate flux for NF of UF permeate, collected during some hours, in recycling experiment. The agitation speed was first set to 1200 rpm, while permeate flux and pollutant rejection were measured at TMP of 0.2–0.6 MPa and these tests were repeated at 100–1200 rpm. For all agitation speeds, the flux increased with TMP lineally, while trended to a stable value after exceeding threshold flux (shown with dot-line). Below threshold flux, fouling rate was almost constant and highly low and flux-TMP was a linear relationship, when flux was higher than threshold flux, fouling rate enhanced with TMP persistently and rate of flux rise reduced [23]. Filtration below threshold flux, due to small impetus, foulant concentration on membrane was low, causing small concentration polarization and foulant deposition on membrane, so fouling rate kept stable and low. However, beyond threshold flux, foulant concentration elevated, and concentration polarization promoted and serious fouling layer formed, leading ever-increasing fouling rate. During NF of wastewater, organic constituents contained in the biologically treated wastewater, such as polysaccharides, proteins, humic and fulvic acids, and nucleic acids, designated as wastewater organic matter, were found to play an important role as membrane foulants, especially the hydrophobic fraction [36]. For Figs. 6 and 7, the amelioration of TMP

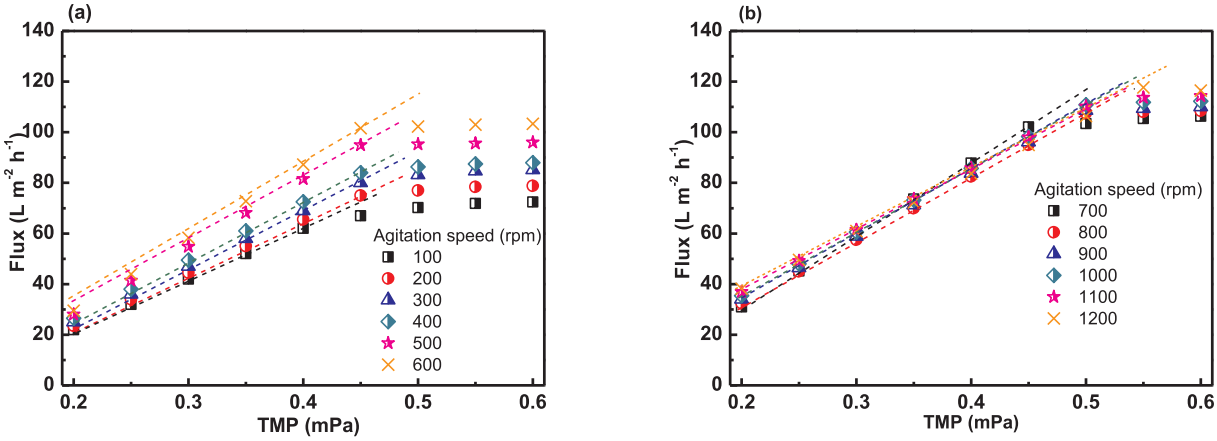

Fig. 5. Nanofiltration flux at different TMPs and agitation speeds.

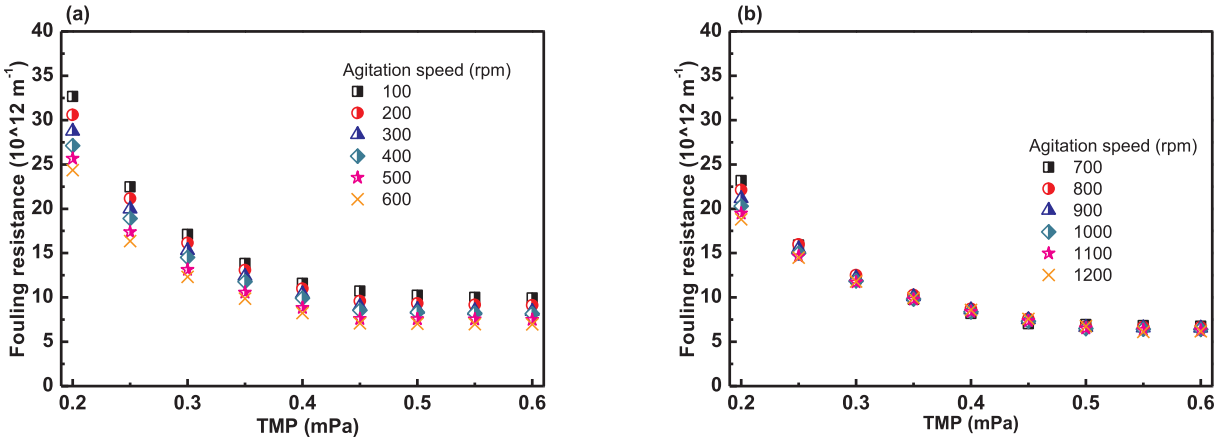

Fig. 6. Nanofiltration fouling resistance at different TMPs and agitation speeds.

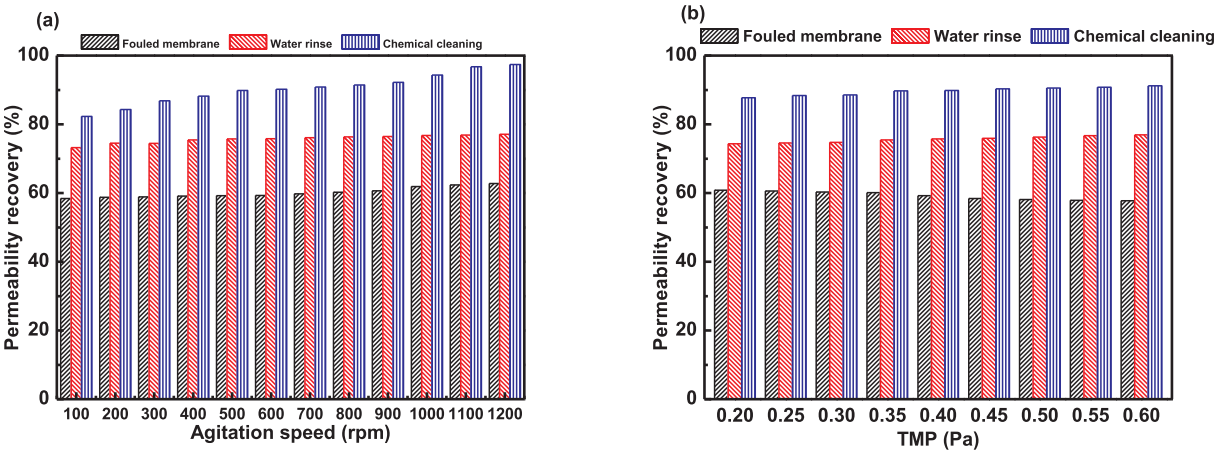

Fig. 7. Nanofiltration cleaning efficiency at different TMPs (a) and agitation speeds (b).

Table 6
Pollutant removal of NF permeate at different shear stresses.

Agitation speed (rpm)	COD (mg/L)	TP (mg/L)	NH_3-N (mg/L)	NO_2-N (mg/L)	NO_3-N (mg/L)
300	4.05	0.22	0.17	0.22	1.48
350	4.01	0.21	0.16	0.18	1.46
400	3.97	0.21	0.15	0.17	1.43
450	3.86	0.20	0.15	0.15	1.39
500	3.68	0.19	0.14	0.14	1.37
550	3.59	0.19	0.14	0.14	1.33
600	3.56	0.17	0.13	0.13	1.29
650	3.54	0.16	0.13	0.13	1.27
700	3.46	0.16	0.11	0.12	1.25
750	3.39	0.15	0.10	0.11	1.24
800	3.32	0.13	0.10	0.11	1.24

diminished the fouling resistance and yet reduced the permeability of fouled membrane, in that higher permeate flux pushed more foulants onto membrane and cut down permeability. After water rinse and chemical cleaning, higher filtration TMP possessed greater permeability recovery, indicating that filtration at higher TMP still owned lower irreversible fouling. For NF of UF permeate, water rinse recovered permeability above 75%, stating that water rinse could break up and clean the fouling layer. The explanation may be that, first, organic molecules in UF permeate were negatively charged, and the electrostatic repulsion among molecules in aggregates made the fouling layer easier to scatter and dissolve in deionized water by water rinse.

Agitation speed, creating a shear stress on membrane, plays an important role for fouling control. At low agitation speed, the lower shear stress and smaller turbulence generated, while the concentration gradient of the retained solutes on the membrane surface formed, bringing about a diffusive transport in the opposite direction from the convective flow of the permeate, and enhancing filtration resistance [37]. Besides, the increment of solute concentration near the membrane caused the raise of viscosity and the formation of a gel layer. If the shear rate was not large enough to remove solutes away from membrane, organic molecules were first adsorbed at membrane surface, then aggregated together due to the hydrophobic interaction [38,39], inducing a continuous flux decline. When agitation speed was increased, flux improved, especially for 100–600 rpm. This result justifies the permeability gain observed previously, and was related to the increased turbulence and shear stress in the region near the membrane. High shear stress dispersed the concentration of retained solutes near the surface of the membrane by decreasing the concentration polarization, which caused foulants deposition on membrane, even including the precipitation of inorganic compounds (scaling) [40]. In addition, greater agitation speed exhibited larger threshold TMP and threshold flux, demonstrating that high fouling rate was controlled by high shear stress, which could also extend limiting regime of membrane operation. Figs. 6 and 7 shows that agitation speed decreases fouling resistance and promotes permeabilities for fouled membrane, water rinse and chemical cleaning, indicating that improved shear stress on membrane surface obviously reduced total fouling resistance, reversible fouling and irreversible fouling. Thus, for NF of UF permeate, elevating hydrodynamic could significantly reinforce fouling control.

Table 6 shows the values of the physicochemical parameters of NF permeates. Improvement in all parameters monitored was noted with the increase in the agitation speed. Because increased shear stress

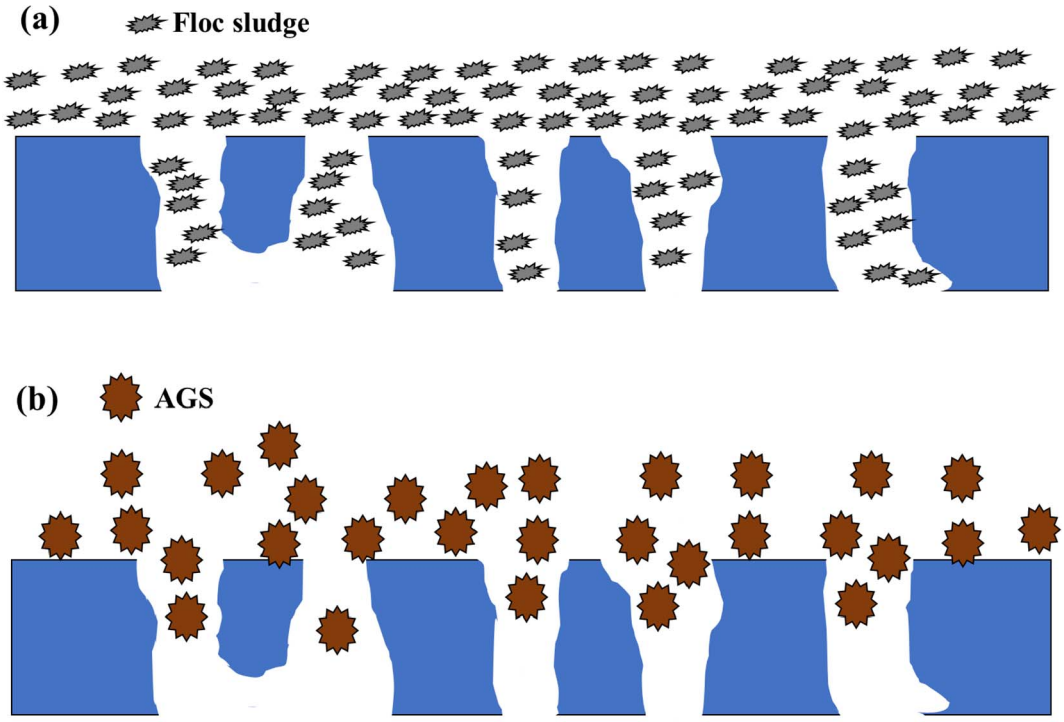

Fig. 8. Schematic diagram of fouling mechanism of floc sludge reactor-UF (a) and AGS reactor-UF (b).

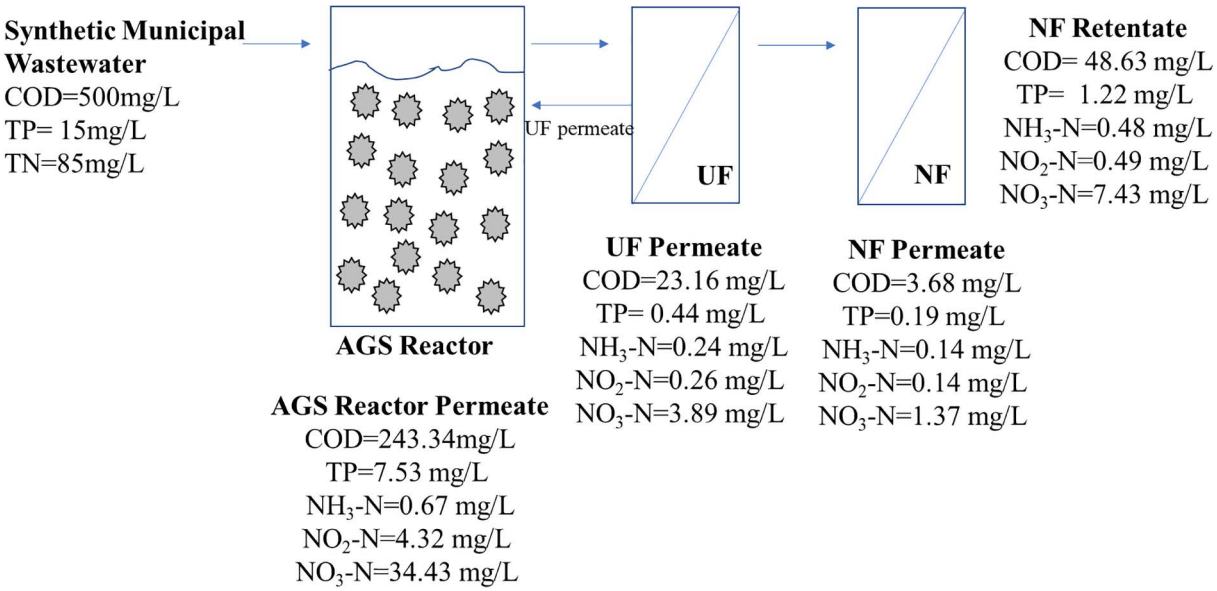

Fig. 9. Pollutant concentration of the raw wastewater, AGS permeate, UF permeate, NF retentate and NF permeate.

decreased the accumulation of solutes rejected on the membrane surface, it also diminished their concentration gradient between the feed and the permeate [36], reducing the driving force for their transport. Besides, because of less fouling at high shear stresses, the passage of solvent was favored, contributing to dilution of the permeate.

4. Discussion

4.1. Membrane fouling mechanism

The main fouling mechanisms for floc sludge reactor-UF and AGS reactor-UF was pore blocking and cake formation. As shown in Fig. 8, for AGS reactor-UF, the main foulants of UF of AGS reactor is aerobic granular sludge, and the most granular sludges are much larger than membrane pore, thus they are almost rejected by membrane. For traditional floc sludge reactor, floc sludge exhibits low size and great varying range. In UF of floc sludge reactor permeate, floc sludge causes serious pore blocking and dense cake layer, because small floc sludges enter membrane pores easily, after that, membrane pores narrow and more floc sludges are retained on membrane, then form cake layer. Due to the great varying range of floc sludge size, its cake layer is more easily compacted and become more and more densely, as well these dense and compacted cake layers present high fouling resistance for UF operation. As for UF of AGS reactor permeate, aerobic granular sludge with larger pore size (size > 100 nm) and dense and stable structure [6], are difficult to enter membrane pores, thus the pore blocking fouling

appears low. Moreover, their cake layer indicates more sparse structure, contributing to low fouling resistance and high flux maintenance. In addition, larger sludge particles own higher hydrophobicity and are conducive to dispersion of foulants by shear stress on membrane. After membrane cleaning, as mentioned at Sections 3.1 and 3.2, permeability could be restored up to 90%. The reason why it cannot reach 100% may be that some stubborn foulants remaining onto membrane can withstand P3-ultrasil 10 cleaning detergent. The next target is to improve cleaning efficiency by using another more suitable cleaning detergent, such as enzyme cleaning agent, or optimizing cleaning condition (shear stress, temperature and time). In general, the cultivation of granular sludge could reinforce membrane fouling control.

4.2. Pollutant removal and water reuse

It is observed that the NF permeate has very low pollutant concentration and meets the standards (COD, TP, NH_3-N, NO_2-N and NO_3-N) for water reuse standards of municipal water and land scape water in China in Fig. 9. The feed quality of NF has a strict requirement [36,41]. In this study, AGS reactor can degrade organic pollutants excellently, because of simultaneous nitrification and denitrification capacity by the aerobic and anoxic environments of granular sludge and the rich microbial community. Together with UF rejection, pollutants can be effectively removed, providing good quality UF effluent for NF feed.

As can be seen in Fig. 9, the overall system efficiencies were very high. It is emphasized that the NF retentate could also be recycled in the industry as reused water for applications that do not require very high quality, such as for irrigating gardens, or could be discarded into bodies of water [42]. The COD concentration of 48.63 mg L^{-1} meets the first grade A standards of Urban Sewage Disposal Plant Contamination Integrated Discharge Standard of China (50 mg COD L^{-1}), thus contributing to the release of better quality effluent and to the preservation of water bodies.

From Fig. 10, there are only some white spots existed on UF or NF membrane surface after experiments, implying that only some foulants distributed on membrane surface and UF and NF membrane still kept at a clean state. The main fouling mechanism was pore blocking and not enough foulants accumulated on membrane, therefore without clear cake layer occurred on membrane. For UF membrane, the large size and mature structure of AGS accounted for the low UF fouling, while for NF membrane, small organic constituents in AGS-UF permeate, including polysaccharides, proteins, humic and fulvic acids, are responsible for low NF fouling.

Fig. 11. shows the FTIR spectrograms of new and cleaning membrane for both UF and NF. Four characteristic peaks (780 cm^{-1}, -(CH_2)n-; 870 cm^{-1}, Penta-substitu Benzene (one hydrogen); 845–880 cm^{-1}, Ar-NO_2; 1100 cm^{-1}, C·OH (Secondary Alcohols); 1545–1560 cm^{-1}, R-NO_2 (acid amides); 1650–1690, $RCONH_2$) of all membrane (fx1) are clearly observed. Compared with the new membrane, the larger peaks of carbon-containing group (780 cm^{-1}, -(CH_2)n-; 870 cm^{-1}, Penta-substitu Benzene (one hydrogen); 1100 cm^{-1}, C·OH (Secondary Alcohols)) and nitrogen-containing groups (845–880 cm^{-1}, Ar-NO_2; 1545–1560 cm^{-1}, R-NO_2 (acid amides); 1650–1690, $RCONH_2$) on the cleaning membrane demonstrate the existence of substances that contain carbon and nitrogen on the fouling layer of membrane, which are MBR foulants. Besides, some of them belong to irreversible fouling and still retain onto membrane after membrane cleaning, indicating that membrane cleaning agent needs to be improved.

Membrane surface morphology and roughness was determined using the non-contact mode AFM. AFM images of the new, fouled and cleaning membrane surfaces for both UF and NF are presented in Fig. 12. The unique ridge and valley shape was observed on the virgin membrane. The resolution of this image is given in the set with scan area of 5 μm × 5 μm. The average roughness of the new membrane surface was 30.4 and 44.1 nm for UF and NF, respectively. After fouled by MBR foulants (mainly granular sludges), the roughness increased up

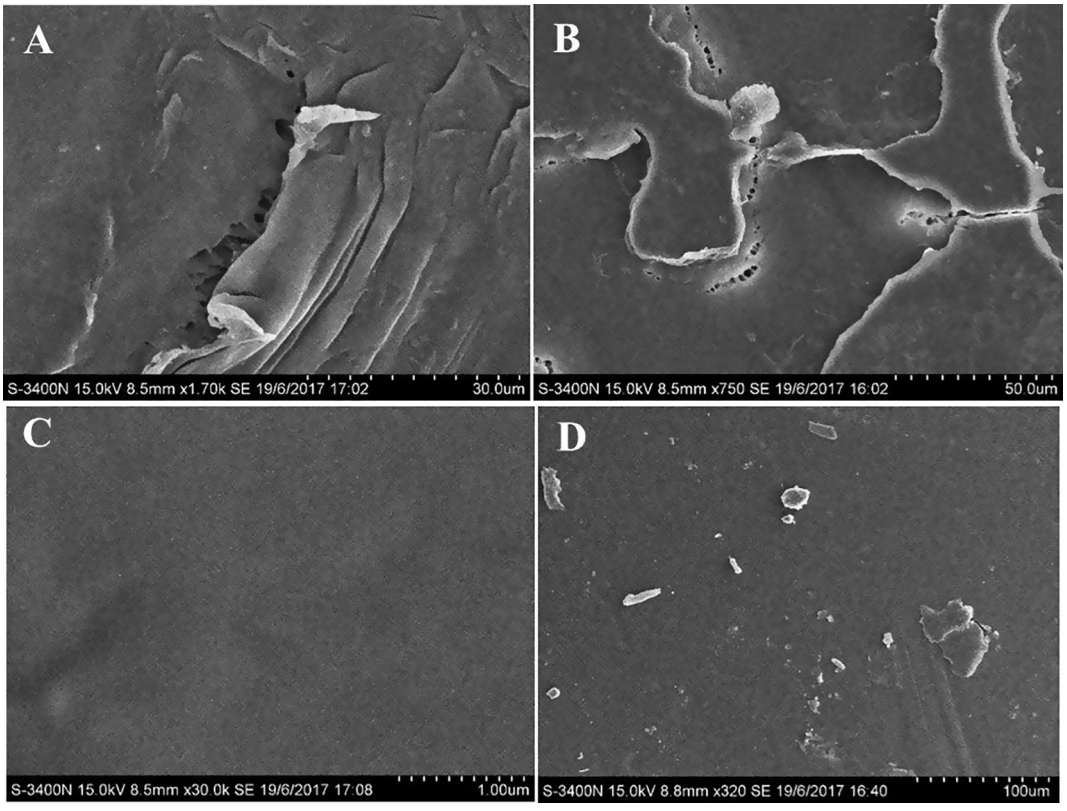

Fig. 10. SEM images of the pristine UF membrane (A), fouled UF membrane (B), pristine NF membrane (C) and fouled NF membrane (D).

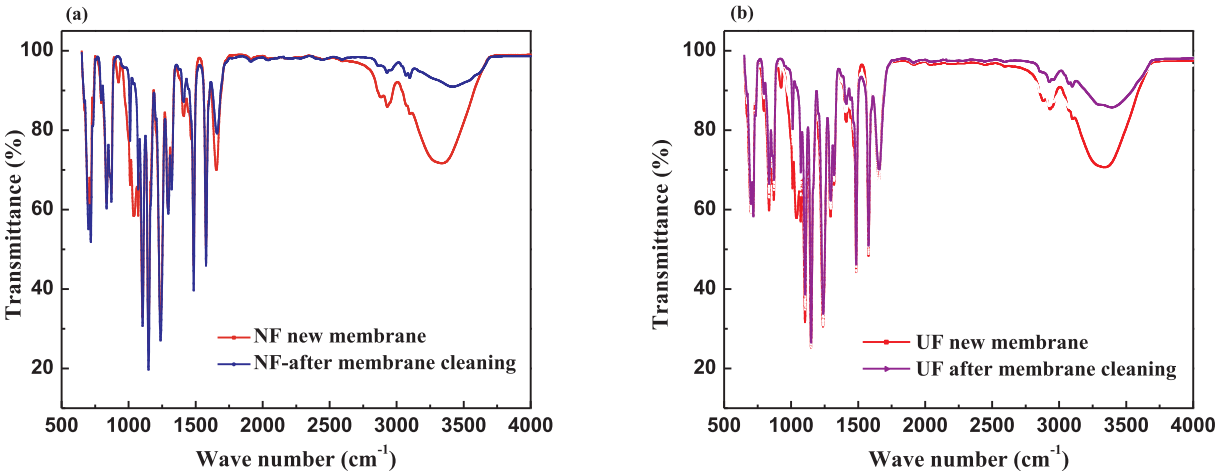

Fig. 11. ATR-FTIR spectrums of new and cleaning membranes.

to 65.8 and 157.7 nm. After membrane cleaning, the roughness decreased to 40.2 and 130.0 nm. Because the accumulation of foulants on membrane enhanced the average roughness, while membrane cleaning removed some part of fouling layer and cut down the average roughness. Furthermore, compared with UF, the increment of roughness of NF membrane after experiment reduced, due to the less foulants on NF membrane.

5. Conclusion

The integrated AGS and UF + NF process is a viable system for treating municipal wastewater, providing high removal efficiencies for organic matter and nutrients: the AGS reactor as primary treatment: COD 51.33%, TN 53.63% and 49.08% TP; UF as secondary treatment: COD 90.48%, TN 94.84% and TP 97.07%; and nanofiltration (NF) as tertiary treatment: COD 99.26%, TN 98.06% and TP 98.73%. After the entire treatment process, the NF permeate demonstrated high quality for water reuse.

For UF and NF, shear stress created by agitation speed played a significant role for fouling control. It not only effectively improved permeate flux, but also reduced fouling resistance, as well as membrane cleaning efficiency was obviously promoted. At 1200 rpm agitation speed of UF and 800 rpm agitation speed of NF, permeate flux was increased to 226.01 $L\,m^{-2}h^{-1}$ for UF and 116.43 $L\,m^{-2}h^{-1}$ for NF,

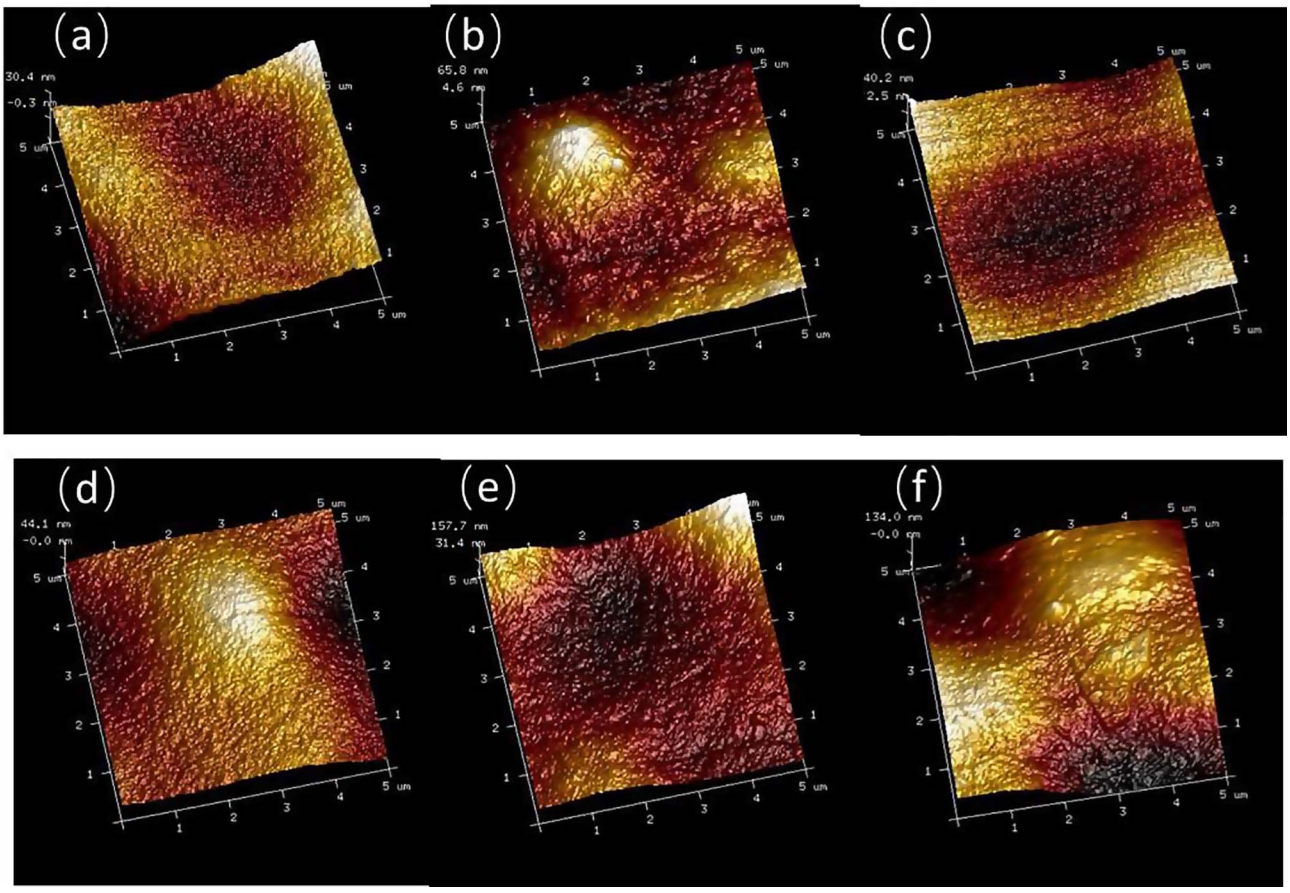

Fig. 12. AFM images and roughness on new (a), fouled (b), and cleaning (c) NF membranes and new (d), fouled (e), and cleaning (f) UF membranes.

fouling resistance was reduced to $3.97 \times 10^{-12}\,m^{-1}$ for UF and $6.17 \times 10^{-12}\,m^{-1}$ for NF, and permeability recovery after membrane cleaning was up to 91.23% for UF and 97.4% for NF. On the other hand, the large size and mature structure of AGS also led to less foulant deposition on membrane and less foulant adsorption into membrane pores than conventional floc sludge. Additionally, the fouling mechanisms of conventional floc sludge and AGS was deeply analyzed and compared, as well as the efficiencies of pollutant treatment and reuse water production for the entire integrated AGS and UF + NF process were revealed. In addition, SEM, ATR-FTIR and AFM were used to analyze membrane fouling. In summary, the results demonstrated an alternative option for water treatment and reuse water production in the integrated AGS and membrane process.

Acknowledgements

The authors would like to acknowledge the financial support from the National Natural Science Foundation of China (No. 41371473), Guangdong Provincial Science and Technology Plan (2016A050503041), Guangdong Natural Science Foundation of China (Grant number 2017A030310540), Guangdong provincial education department Youth Innovative Talents Project (Grant 17ZK0110), Scientific Research Fund of Guangdong University of Technology (Grant 220413582) and National Natural Science Foundation of China (No. 21476050). Dr. Zhang would specifically like to highlight the invaluable support received from his wife Lili Shi.

Appendix A. Supplementary data

Supplementary data associated with this article can be found, in the online version, at http://dx.doi.org/10.1016/j.cej.2017.12.078.

References

[1] X.W. Liu, G.P. Sheng, H.Q. Yu, Physicochemical characteristics of microbial granules, Biotechnol. Adv. 27 (2009) 1061–1070.
[2] M. Pronk, M.K. de Kreuk, B.B. De, P. Kamminga, R. Kleerebezem, M.C. van Loosdrecht, Full scale performance of the aerobic granular sludge process for sewage treatment, Water Res. 84 (2015) 207.
[3] J. Zhao, J. Huang, M. Guan, Y. Zhao, G. Chen, X. Tian, Mathematical simulating the process of aerobic granular sludge treating high carbon and nitrogen concentration wastewater, Chem. Eng. J. 306 (2016) 676–684.
[4] Z. Zhu, Q. Wu, X. Di, S. Li, F.J. Barba, M. Koubaa, S. Roohinejad, X. Xiong, J. He, Multistage recovery process of seaweed pigments: investigation of ultrasound assisted extraction and ultra-filtration performances, Food Bioprod. Process. 104 (2017).
[5] A. Scalia, F. Bella, A. Lamberti, S. Bianco, C. Gerbaldi, E. Tresso, C.F. Pirri, A flexible and portable powerpack by solid-state supercapacitor and dye-sensitized solar cell integration, J. Power Sources 359 (2017).
[6] C. Chen, L. Bin, B. Tang, S. Huang, F. Fu, Q. Chen, L. Wu, C. Wu, Cultivating granular sludge directly in a continuous-flow membrane bioreactor with internal circulation, Chem. Eng. J. 309 (2016) 108–117.
[7] A.M. Lotito, M.D. Sanctis, C.D. Iaconi, G. Bergna, Textile wastewater treatment: aerobic granular sludge vs activated sludge systems, Water Res. 54 (2014) 337–346.
[8] S.J. Lim, T.H. Kim, Applicability and trends of anaerobic granular sludge treatment processes, Biomass Bioenergy 60 (2014) 189–202.
[9] W. Zhang, J. Luo, L. Ding, M.Y. Jaffrin. A Review on Flux Decline Control Strategies in Pressure-Driven Membrane Processes, in: Proceedings of the 4th International Conference on Foundations of Software Science and Computation Structures, 2015. pp. 303–317.
[10] W. Zhang, L. Ding, Investigation of membrane fouling mechanisms using blocking models in the case of shear-enhanced ultrafiltration, Sep. Purif. Technol. 141 (2015) 160–169.
[11] J. Luo, Y. Wan, Effects of pH and salt on nanofiltration—a critical review, J. Membr. Sci. 438 (2013) 18–28.
[12] W. Gao, H. Liang, J. Ma, M. Han, Z.L. Chen, Z.S. Han, G.B. Li, Membrane fouling control in ultrafiltration technology for drinking water production: a review, Desalination 272 (2011) 1–8.
[13] W. Zhang, L. Ding, J. Luo, M.Y. Jaffrin, B. Tang, Membrane fouling in photocatalytic membrane reactors (PMRs) for water and wastewater treatment: a critical review, Chem. Eng. J. 302 (2016) 446–458.
[14] X. Li, F. Gao, Z. Hua, G. Du, J. Chen, Treatment of synthetic wastewater by a novel MBR with granular sludge developed for controlling membrane fouling, Sep. Purif. Technol. 46 (2005) 19–25.
[15] F. Meng, S.R. Chae, A. Drews, M. Kraume, H.S. Shin, F. Yang, Recent advances in membrane bioreactors (MBRs): membrane fouling and membrane material, Water Res. 43 (2009) 1489.
[16] C. Boaretti, L. Pasquini, R. Sood, S. Giancola, A. Donnadio, M. Roso, M. Modesti, S. Cavaliere, Mechanically stable nanofibrous sPEEK/Aquivion®; composite membranes for fuel cell applications, J. Membr. Sci. (2017).
[17] J.H. Tay, P. Yang, W.Q. Zhuang, S.T.L. Tay, Z.H. Pan, Reactor performance and membrane filtration in aerobic granular sludge membrane bioreactor, J Membr. Sci. 304 (2007) 24–32.
[18] F. Meng, S. Zhang, Y. Oh, Z. Zhou, H.S. Shin, S.R. Chae, Fouling in membrane bioreactors: an updated review, Water Res. 114 (2017) 151.
[19] F. Colò, F. Bella, J.R. Nair, C. Gerbaldi, Light-cured polymer electrolytes for safe, low-cost and sustainable sodium-ion batteries, J. Power Sources 365 (2017) 293–302.
[20] T. Xiang, Z. Sheng, L.R. Xu, M.C. Zhang, J.R. Zhu, Performance and fouling characteristics in a membrane sequence batch reactor (MSBR) system coupled with aerobic granular sludge, Desalination 261 (2010) 191–196.
[21] B.X. Thanh, C. Visvanathan, M. Spérandio, R.B. Aim, Fouling characterization in aerobic granulation coupled baffled membrane separation unit, J. Membr. Sci. 318 (2008) 334–339.
[22] B.T.G.C. Luying Wu, Co-existence of diverse sludge granules in a single membrane bioreactor, Chem. Eng. J. 326 (2017) 849–852.
[23] R.W. Field, G.K. Pearce, Critical, sustainable and threshold fluxes for membrane filtration with water industry applications, Adv. Colloid Interface Sci. 164 (2011) 38.
[24] W. Zhang, L. Ding, Z. Zhang, J. Wei, M.Y. Jaffrin, G. Huang, Threshold Flux and Limiting Flux for Micellar Enhanced Ultrafiltration as Affected by Feed Water: Experimental and Modeling Studies, J. Clean Prod. 112 (2016).
[25] N°. Standard Methods for the Examination of Water and Wastewater, 21st Edition. Journal - American Water Works Association, 2006, pp. 130.
[26] N.O. Becht, D.J. Malik, E.S. Tarleton, Evaluation and comparison of protein ultrafiltration test results: dead-end stirred cell compared with a cross-flow system, Sep. Purif. Technol. 62 (2008) 228–239.
[27] K. Xiao, Y. Shen, X. Huang, An analytical model for membrane fouling evolution associated with gel layer growth during constant pressure stirred dead-end filtration, J. Membr. Sci. 427 (2013) 139–149.
[28] K. Xiao, X. Wang, X. Huang, T.D. Waite, X. Wen, Analysis of polysaccharide, protein and humic acid retention by microfiltration membranes using Thomas' dynamic adsorption model, J. Membr. Sci. 342 (2010) 22–34.
[29] J. Luo, A.S. Meyer, G. Jonsson, M. Pinelo, Enzyme immobilization by fouling in ultrafiltration membranes: impact of membrane configuration and type on flux behavior and biocatalytic conversion efficacy, Biochem. Eng. J. 83 (2014) 79–89.
[30] W. Zhang, N. Grimi, M.Y. Jaffrin, L. Ding, Leaf protein concentration of alfalfa juice by membrane technology, J. Membr. Sci. 489 (2015) 183–193.
[31] W. Zhang, Z. Zhu, M.Y. Jaffrin, L. Ding, Effects of hydraulic conditions on effluent quality, flux behavior, and energy consumption in a shear-enhanced membrane filtration using Box-Behnken response surface methodology, Ind. Eng. Chem. Res. 53 (2014) 7176–7185.
[32] J. Luo, L. Ding, Y. Wan, M.Y. Jaffrin, Threshold flux for shear-enhanced nanofiltration: experimental observation in dairy wastewater treatment, J. Membr. Sci. 409–410 (2012) 276–284.
[33] J. Luo, L. Ding, B. Qi, M.Y. Jaffrin, Y. Wan, A two-stage ultrafiltration and nanofiltration process for recycling dairy wastewater, Bioresour. Technol. 102 (2011) 7437–7442.
[34] A. Ding, H. Liang, G. Li, N. Derlon, I. Szivak, E. Morgenroth, W. Pronk, Impact of aeration shear stress on permeate flux and fouling layer properties in a low pressure membrane bioreactor for the treatment of grey water, J. Membr. Sci. 510 (2016) 382–390.
[35] H. Wang, F. Qu, A. Ding, H. Liang, R. Jia, K. Li, L. Bai, H. Chang, G. Li, Combined effects of PAC adsorption and in situ chlorination on membrane fouling in a pilot-scale coagulation and ultrafiltration process, Chem. Eng. J. 283 (2016) 1374–1383.
[36] L.H. Andrade, F.D.S. Mendes, J.C. Espindola, M.C.S. Amaral, Nanofiltration as tertiary treatment for the reuse of dairy wastewater treated by membrane bioreactor, Sep. Purif. Technol. 126 (2014) 21–29.
[37] J. Lin, W. Ye, H. Zeng, H. Yang, J. Shen, S. Darvishmanesh, P. Luis, A. Sotto, B.V.D. Bruggen, Fractionation of direct dyes and salts in aqueous solution using loose nanofiltration membranes, J. Membr. Sci. 477 (2015) 183–193.
[38] J. Fan, J. Luo, Y. Wan, Aquatic micro-pollutants removal with a biocatalytic membrane prepared by metal chelating affinity membrane chromatography, Chem. Eng. J. (2017).
[39] J. Luo, L. Ding, Y. Wan, P. Paullier, M.Y. Jaffrin, Application of NF-RDM (nanofiltration rotating disk membrane) module under extreme hydraulic conditions for the treatment of dairy wastewater, Chem. Eng. J. 163 (2009) 307–316.
[40] J. Lin, W. Ye, J. Huang, B. Ricard, M.C. Baltaru, B. Greydanus, S. Balta, J. Shen, M. Vlad, A. Sotto, Toward resource recovery from textile wastewater: dye extraction, water and base/acid regeneration using a hybrid NF-BMED process, ACS Sustainable Chem. Eng. 9 (2015) 1993–2001.
[41] A.A. Alturki, N. Tadkaew, J.A. Mcdonald, S.J. Khan, W.E. Price, D.N. Long, Combining MBR and NF/RO membrane filtration for the removal of trace organics in indirect potable water reuse applications, J. Membr. Sci. 365 (2010) 206–215.
[42] J. Wang, K. Li, Y. Wei, Y. Cheng, D. Wei, M. Li, Performance and fate of organics in a pilot MBR-NF for treating antibiotic production wastewater with recycling NF concentrate, Chemosphere 121 (2015) 92–100.